Available online at www.sciencedirect.com
ScienceDirect
Trans. Nonferrous Met. Soc. China 29(2019) 1864−1872
Transactions of Nonferrous Metals Society of China
www.tnmsc.cn

Microstructure and mechanical properties of TIG/A-TIG welded AZ61/ZK60 magnesium alloy joints

Bo QIN[1,2], Fu-cheng YIN[1], Cheng-zong ZENG[3], Jia-cheng XIE[3], Jun SHEN[3]

1. School of Materials Science and Engineering, Xiangtan University, Xiangtan 411105, China;
2. Hunan Provincial Key Laboratory of Vehicle Power and Transmission System, Hunan Institute of Engineering, Xiangtan 411104, China;
3. National Engineering Research Center for Magnesium Alloys, College of Material Science and Engineering, Chongqing University, Chongqing 400044, China

Received 25 December 2018; accepted 21 May 2019

Abstract: The dissimilar joints of AZ61 and ZK60 magnesium alloys were obtained by tungsten inert gas arc (TIG) welding and activating tungsten inert gas arc (A-TIG) welding processes. Microstructure characterization shows that, the fine α-Mg equiaxed dendrite crystals contained $Mg_{17}Al_{12}$ and $MgZn_2$ particles in the fusion zone. The average size of the α-Mg grains in the fusion zone was refined to 19 μm at welding current of 80 A, which resulted in the largest tensile strength of 207 MPa. The tensile strength and the width of the beam of the A-TIG welded AZ61/ZK60 joints showed strong dependence on the amount of TiO_2. However, the inhomogeneity of the heat-affected zone near different base metals presented no significant effect on the mechanical properties of the welded joint.

Key words: AZ61; ZK60; dissimilar joints; tungsten inert gas arc (TIG) welding; activating tungsten inert gas arc (A-TIG) welding; inhomogeneity

1 Introduction

Magnesium alloys have attracted tremendous interests and potential applications in lightweight structure manufacturing due to their low density, high specific strength, excellent castability, and good thermal conductivity [1−4]. Due to the fact that the welding of magnesium alloy joints is difficult, the applications of complex structural components of the magnesium alloy are limited. For example, the pores and hot cracks as well as welding deformation occur during the welding process of magnesium alloy and then degrade the mechanical properties of the joints [5]. In order to obtain a high-quality magnesium alloy welded joint, reliable and effective welding technologies have been developed for magnesium alloys in recent years [6,7].

So far, numerous experimental studies concerning the welding technique for the joining of magnesium alloys have been reported [8–10]. The developed welding methods include laser welding [11], friction stir welding [12], and laser−tungsten inert gas hybrid welding [13]. Due to its great flexibility, adaptability and controllability, tungsten inert gas arc (TIG) welding has been demonstrated to be an efficacious way to form high quality welding joints of magnesium alloys [14]. For example, SHEN and XU [15] studied the effects of preheat treatments on the microstructures and mechanical behaviors of AZ61 magnesium alloy joints by the TIG welding. The results indicated a positive correlation between the microhardness of the fusion zone (FZ) and the ultimate tensile strength of the welded joints with the preheat process. In addition, the TIG welding technology integrated with the long-wave ultraviolet A (UVA) treatment promoted the grain refinement of the magnesium alloy joints [16]. YANG et al [17] reported the effects of ultrasonic vibration-assisted TIG welding on the microstructures and mechanical properties of MB3/AZ31 dissimilar magnesium alloy joints. Welding pores were eliminated and the α-Mg grains in the fusion zone were defined by the UVA treatment. However, few systematic studies have focused on the inhomogeneity of

Foundation item: Project (51771160) supported by the National Natural Science Foundation of China; Project (2018JJ4048) supported by the Provincial and Municipal Joint Fund for Natural Science of Hunan Province, China
Corresponding author: Fu-cheng YIN; Tel: +86-731-58298428; E-mail: fuchengyin@xtu.edu.cn
DOI: 10.1016/S1003-6326(19)65094-6

the microstructures and mechanical properties of TIG-welded dissimilar joints. It is expected that such studies will contribute to optimizing the processing parameters for the development of high-performance magnesium alloy structural components.

Although high-quality TIG-welded magnesium alloy joints have been obtained in the researches, well-welded dissimilar magnesium alloys by an activating TIG (A-TIG) welding technology are currently scarce. Potential problems such as molten pool deflection and uneven mechanical properties may exist between dissimilar magnesium alloys due to their compositional differences [18,19]. Therefore, research on the joining of dissimilar magnesium alloys by an A-TIG welding process is technologically important for practical uses and applications. So, the present study is focused on the AZ61/ZK60 dissimilar magnesium alloy joints prepared by TIG and A-TIG welding technology. The tensile strength, microhardness, microstructure, and phase composition of the dissimilar wrought magnesium alloy welded joints were systematically investigated. The relationship between compositional differences and joint performances of the A-TIG welded AZ61/ZK60 dissimilar magnesium alloy joints was also discussed in details.

2 Experimental

AZ61 and ZK60 magnesium alloys were selected as the targets of interest. Both dissimilar magnesium alloy plates were cut into specimens with dimensions of 80 mm × 40 mm × 3 mm for the TIG/A-TIG welding tests. The chemical composition of the alloy is given in Table 1. A differential scanning calorimeter (DSC; DSC404F3) was utilized to analyze the solidus and liquidus temperatures of the AZ61 and ZK60 magnesium alloys. Each sample was heated in a temperature range from 300 to 973 K and held for 10 min. Finally, the samples were cooled to room temperature at a cooling rate of 10 K/min.

Table 1 Nominal chemical compositions of AZ61 and ZK60 magnesium alloy plates (wt.%)

Alloy	Al	Zn	Zr	Mn	Cu	Mg
AZ61	5.8	1	−	0.18	0.003	Bal.
ZK60	−	5.5−6.0	>0.45	−	−	Bal.

Before welding, the surfaces of the samples were polished to 800 grit using SiC sandpaper and then decreased with acetone. For A-TIG welding, TiO_2 particles were pre-coated on the magnesium alloy plates. Dissimilar magnesium alloy samples were fixed on the steel plate and then welded under the TIG condition of AVP−360 welding machine. A distance of 2 mm was maintained between the tungsten pole and the surface of the magnesium alloy plates. The welding process adopted 99.99% argon gas flow at a flow rate of 7.5 L/min. Welding speed was held at 180 mm/min, and the heat input of the welding process was changed by adjusting the welding current (I), as listed in Table 2.

Table 2 Applied welding parameters

Sample	1	2	3	4	5
Welding current/A	60	70	80	90	100

Welded samples with good weld appearances were chosen for further testing. Prior to tests, the cross-sections of the welded samples were polished to 3000 grit and etched with a solution containing about 10 mL of picric acid, about 2 mL of ethyl alcohol, and about 3 mL of acetic acid in distilled water for 10−20 s. The microstructural features and morphology were analyzed by optical microscopy (Axiovert A1, OM) and a scanning electron microscopy (SEM; VEGA 3 LMH). The phases formed in the welded seams were characterized using an X-ray diffraction system (Empryean) and through an energy dispersive X-ray spectroscopy (EDS; OXFORD, Inc. ISIS300). Selected welded samples were cut into dog-bone shape for tensile strength measurement tests, which were carried out by using a tensile test machine (SANS XYA105C) under a velocity of 1 mm/min at room temperature. The microhardness of the cross-sections were then determined using a Vickers hardness tester (V−1000) in a period of 20 s, with a load of 0.49 N and a step size of 0.5 mm.

3 Results and discussion

3.1 Microstructural analysis

Figure 1 presents the microstructures of the AZ61/ZK60 TIG welded joints. The magnesium alloy base metal, heat affected zone (HAZ), and the fusion zone (FZ) are separated by the fusion line. On the side of AZ61, the HAZ exhibited larger grains and the FZ presented more refined grains as compared to the grains of the AZ61 base metal. The evolution of the grains on the side of ZK60 was similar to that on the side of AZ61 alloy. The microstructure of the AZ61/ZK60 joints consisted of α-Mg phase and secondary phase. Small equiaxed dendritic crystals and secondary phase were observed in the FZ also. An inverse correlation was observed between the quantity of the secondary phase (black particles) and the decreasing distance from FZ. A portion of the secondary phase precipitated as divorced eutectic during the solidification of the liquid phase, and

then the remaining portion was generated due to the solid phase transformation of the α-Mg matrix after solidification [9].

Figures 2(a−e) show the microstructures of the FZ of the AZ61/ZK60 magnesium alloy welded seams at different welding currents. The FZ presented fine equiaxed grains and dispersed globular or lamellar-like secondary phase particles [11,20]. A positive correlation was observed between the welding current and both the secondary phase particle sizes and the solidification time of the magnesium alloy weld pool, thus resulting in the increased precipitation of secondary phase particles during solidification. This feature indicates that the secondary phase particles in the FZ primarily generated through the solidification of the liquid phase. The average size of the grains in the FZ performed at varying welding currents was measured (Image J) and the results are presented in Fig. 2(f). The size of the grains in the FZ initially decreased with the increase of welding current and attained a minimum value at 80 A, and then increased with further increase in the welding current, which indicated that the grain size of the FZ was greatly refined at the welding current of 80 A. The refined grain size in the FZ of the TIG welded AZ61/ZK60 magnesium alloy joints was evaluated to be about 19 μm. In fact, the grain size in the FZ mainly depended on the synergistic effect of the cooling rate and the heat input. The cooling rate dominated the refinement of the grain size as the welding current was decreased to a level below 80 A. Conversely, the heat input became the main factor for the grains size evolution in the case of the welding current exceeding 80 A. These two factors reached a compromise at a welding current of 80 A. In addition, due to the high cooling rate, more secondary

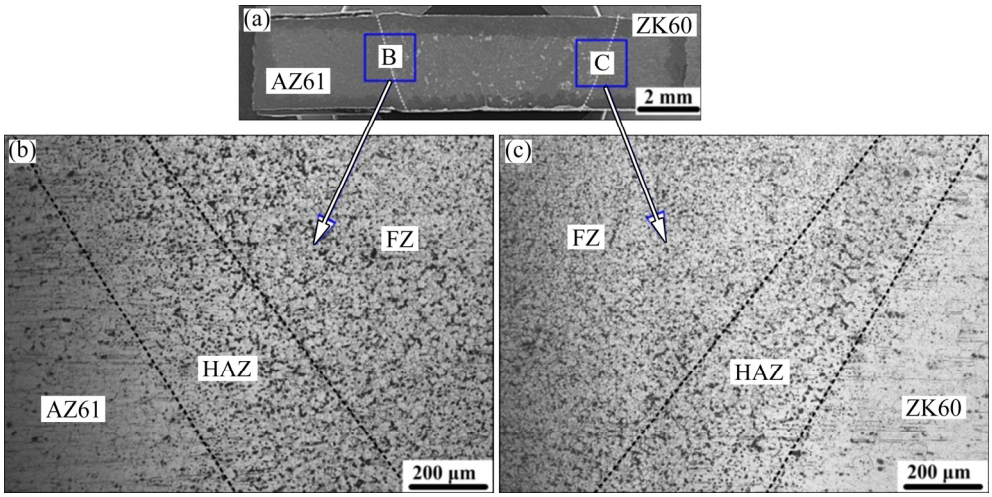

Fig. 1 Typical structure of TIG welded AZ61/ZK60 magnesium alloy joints at welding current of 80 A: (a) Macroscopic joint image; (b) Transition zone near AZ61 base metal; (c) Transition zone near ZK60 base metal

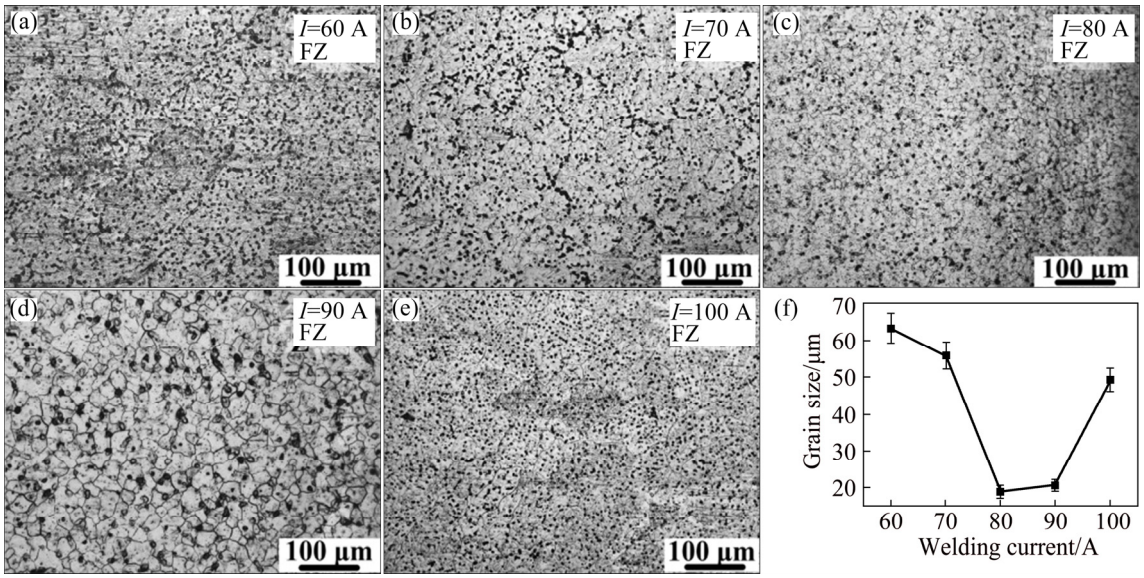

Fig. 2 Microstructural images in FZ of TIG welded AZ61/ZK60 magnesium alloy joints at different welding current levels of 60 A (a), 70 A (b), 80 A (c), 90 A (d), 100 A (e) and corresponding grain size (f)

phase particles were impelled by the segregation of the Al or Zn atoms at the liquid–solid interface. The nucleation of α-Mg and the secondary phase accelerated in this condition, so that the grain size decreased markedly and then the smallest grains formed.

The effect of heat input on the microstructure of the FZ is shown in Figs. 3(a−c). α-Mg in the FZ was identified by fine equiaxed dendrites with surrounding secondary phase. At a welding current of 80 A, more secondary phase particles were observed in the FZ, as shown in Fig. 3(b). The microstructures of the AZ61 and ZK60 base metals are presented in Figs. 3(d) and (e), respectively. And the secondary phase in AZ61 and ZK60 was $Mg_{17}Al_{12}$ (white particles) and $MgZn_2$ (gray particles), respectively. Both the $Mg_{17}Al_{12}$ and $MgZn_2$ phases were observed in the FZ of the TIG welded AZ61/ZK60 joints. Furthermore, the amount of the secondary phase in the FZ was more than that in the base metal (either AZ61 or ZK60). Given that the FZ underwent melting and solidification, the formed $Mg_{17}Al_{12}$ particles distributed along the grain boundaries of α-Mg during solidification. A high welded seam temperature was maintained during solidification, thereby precipitating $Mg_{17}Al_{12}$ particles in the base metal until the temperature decreased to a level below the transition temperature. The $MgZn_2$ particles were performed in the same process. Also, the number of secondary phase particles was influenced by the nucleation rate, which was associated with the solid-state phase transformation driving force, solid-state phase transformation resistance, and Al atom diffusion rate [21]. The driving force of the solid-state phase transformation enhanced as the cooling rate reached its maximum value (welding current of 80 A). Thereby, this promoted the nucleation of more secondary phase particles. Hence, more secondary phase particles were found in the FZ as the welding current was set at 80 A. To determine the composition of the secondary phase particles in the welded joints at a welding current of 80 A, the element distribution across the fracture was recorded by linear EDS (Fig. 3(f)). The relative intensity of the Mg element was obviously inversely correlated with increasing distance from the central FZ, which indicated that the α-Mg phase content decreased at farther distances from the central FZ. As previously mentioned, α-Mg in the FZ was surrounded by a secondary phase. Hence, it can be assumed that the amount of secondary phase in the welded joints increased with decreasing distance from the central FZ.

The amounts of $Mg_{17}Al_{12}$ particles and the $MgZn_2$ particles are different in the FZ. SHI et al [22] reported that if the magnesium−aluminum binary solution is a regular solution with infinite dilutions, the interaction coefficient of the two metals can be estimated by the enthalpy of mixing. The enthalpy of mixing can be expressed as $\lambda_{ij}=(\overline{\Delta H}^{\infty}_{i(j)}+\overline{\Delta H}^{\infty}_{j(i)})/2$, where $\overline{\Delta H}^{\infty}_{i(j)}$ is the enthalpy of mixing of i in j, and $\overline{\Delta H}^{\infty}_{j(i)}$ is the enthalpy of mixing of j in i. As reported by ZHANG et al [23], the interaction coefficient of magnesium and aluminum is λ_{Mg-Al}=−4.764 kJ/mol. In this study, the

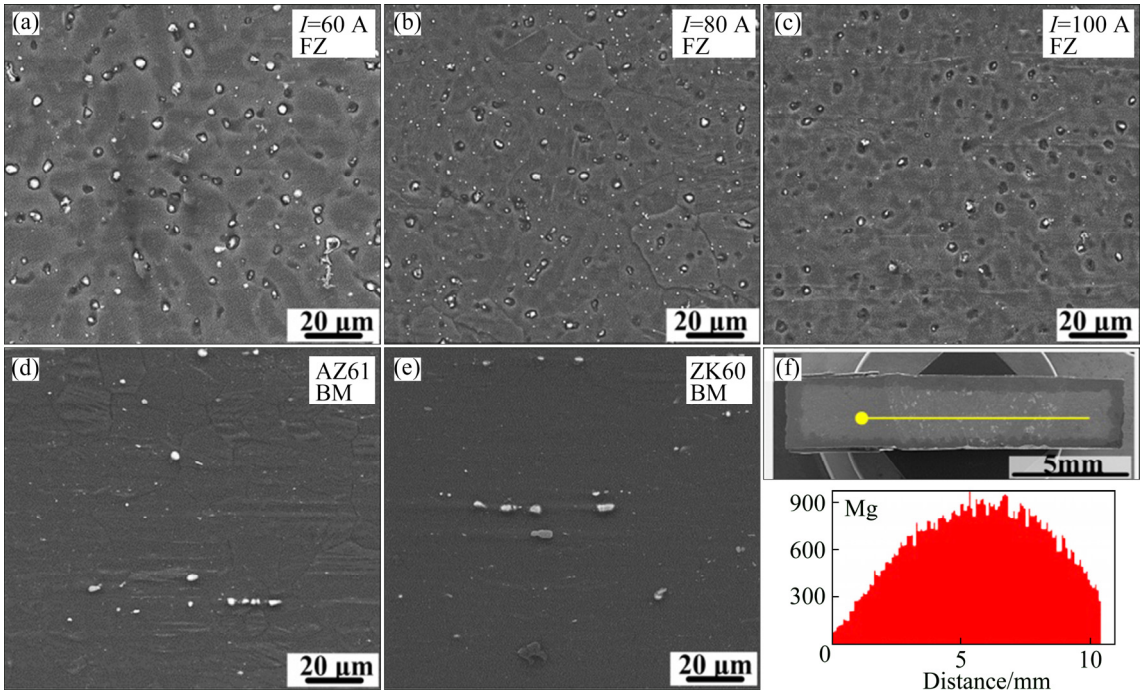

Fig. 3 SEM images of FZ at welding currents of 60 A (a), 80 A (b) and 100 A (c), AZ61 (d) and ZK60 (e) magnesium alloy, and relative amount of Mg varied from AZ61 to ZK60 at welding current of 80 A (f)

interaction coefficient of magnesium and zinc can be calculated as λ_{Mg-Al}=−7.272 kJ/mol. Since the affinity of the two metals is reflected by the interaction coefficient λ_{ij}, large negative interaction coefficient λ_{ij} indicates a greater affinity between two metals. Therefore, the interaction coefficient of Mg−Al is less than that of Mg−Zn.

3.2 Phase identification

Figure 4 shows the DSC measurement results of the AZ61 and ZK60 magnesium alloys performed at different temperatures. The solidus temperature of the AZ61 magnesium alloy was obtained during the heating process and the liquidus temperature of AZ61 magnesium alloy was measured by the DSC thermogram during the cooling period. So, the molten temperature region of the AZ61 and ZK60 magnesium alloys could be determined. The results indicated that the molten temperature region of the ZK60 magnesium alloy was smaller than that of the AZ61 magnesium alloy.

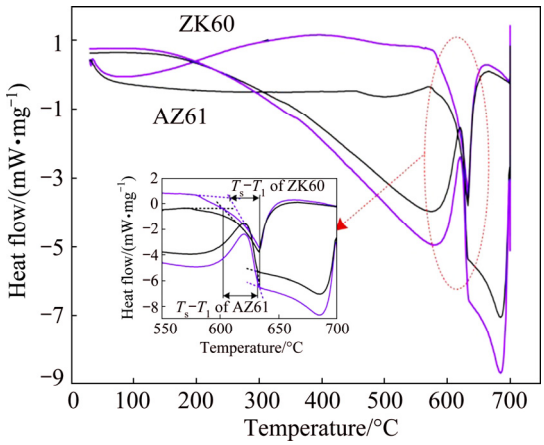

Fig. 4 DSC curves of AZ61 and ZK60 magnesium alloys

The solidus temperature of the AZ61 magnesium alloy was lower than that of the ZK60 magnesium alloy. However, both magnesium alloys exhibited small differences in their liquidus temperatures. This indicated that the AZ61 magnesium alloy had a longer solidification time compared with that of the ZK60 magnesium alloy during welding. As a result, more $Mg_{17}Al_{12}$ particles formed in the molten AZ61 magnesium alloy. Due to the low affinity of the Mg−Al, the AZ61 magnesium alloy around the ZK60 magnesium alloy remained as a liquid when the temperature of the weld beam was below the solidus temperature of the ZK60 magnesium alloy. $MgZn_2$ particles precipitated in the FZ and also the amount of them is similar to that of the $Mg_{17}Al_{12}$ particles.

The secondary phases in the AZ61 magnesium alloy and ZK60 magnesium alloy were identified as $Mg_{17}Al_{12}$ and $MgZn_2$ phases, respectively, by the XRD pattern in Fig. 5. Both the $Mg_{17}Al_{12}$ and $MgZn_2$ phases were observed in the TIG welded AZ61/ZK60 joints. According to the diffraction peak intensities of the welded joints (either AZ61 side or ZK60 side), the Mg content in the welded joints decreased compared with that of the magnesium alloy base metal. This is mainly due to the evaporation of Mg during the welding process. The inverse correlation between the intensity of the welded joints and the increase of the welding current suggested that Mg evaporation in the welded seam increased with the increase of the welding current.

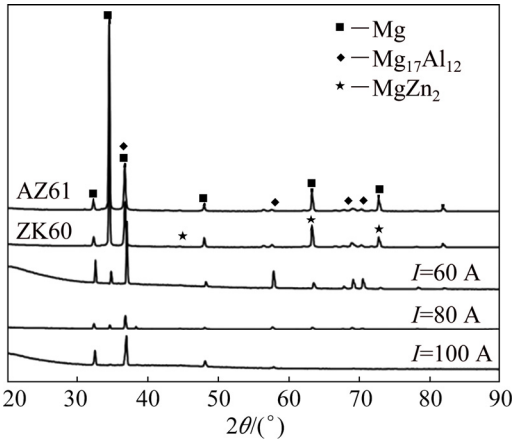

Fig. 5 XRD patterns of base metal and welded joints

3.3 Mechanical properties

Figure 6 shows the tensile strength of the base metals (AZ61 and ZK60) and the TIG welded joints of the dissimilar magnesium alloys as a function of the welding current. The tensile strength of the AZ61/ZK60 welded joints initially presented a positive correlation with the welding current up to its maximum (207 MPa). After that, the tensile strength dropped. The maximum tensile strength was observed at a welding current of 80 A. In addition, tensile strength of ZK60 magnesium alloy was lower than that of the AZ61 magnesium alloy. The tensile strength of TIG welded AZ61/ZK60

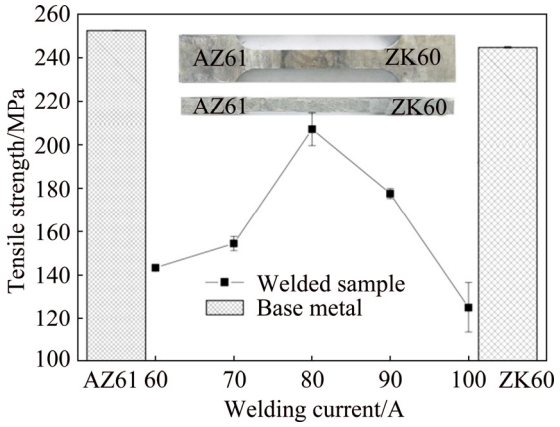

Fig. 6 Tensile strength of base metal and welded joints

magnesium alloy joints at different currents was lower than that of both AZ61 and ZK60 magnesium alloys.

The transverse microhardness distribution of the TIG welded AZ61/ZK60 joints at a welding current of 80 A is shown in Fig. 7(a). The microhardness of the AZ61 magnesium alloy was higher than that of the ZK60 magnesium alloy. The microhardness of the HAZ near the AZ61 or ZK60 magnesium alloys was lower than that of the base metals. Figure 7(b) presents the transverse microhardness of the FZ in a welding current range of 60−100 A. A positive correlation was initially observed between the microhardness of the FZ and welding current until the welding current arrived to 80 A. After that, the microhardness deceased with the increase of the welding current.

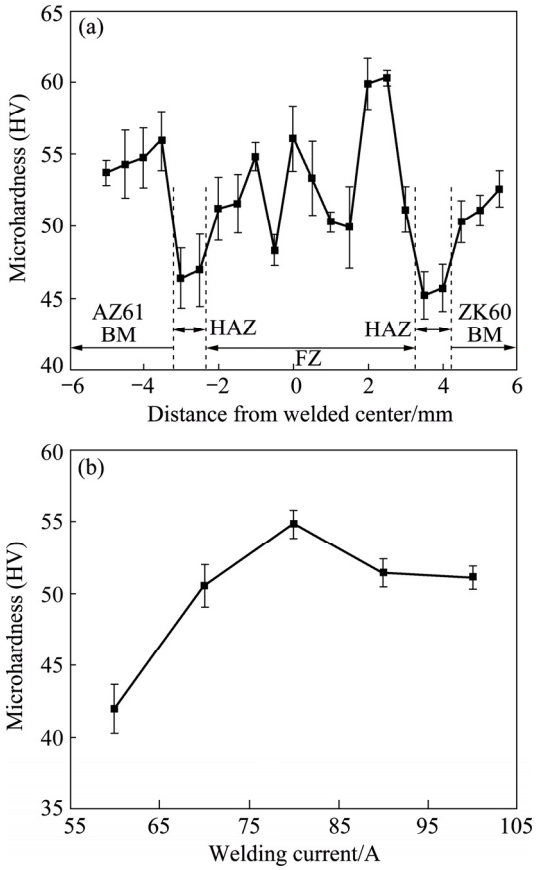

Fig. 7 Microhardness across weld cross-section at welding current of 80 A (a) and microhardness of FZ at different welding currents (b)

As discussed in Section 3.1, the grains of the FZ were refined under a welding current of 80 A, and then the microhardness of the welded joints was increased. When the welding current exceeded 80 A, grain coarsening caused the microhardness of the welded joints to decrease due to slow heat dissipation at high heat input.

The microstructures of the A-TIG welded AZ61/ZK60 joints are shown in Fig. 8. A significant difference was observed in the microstructure of the transition zone near different magnesium alloy base metals. The HAZ near the ZK60 side was wider than that near the AZ61 side. This is because the active flux-induced deflection of the molten pool enhanced the heat input on one side of the joint. Moreover, the phase distribution generated local unevenness in the A-TIG welded AZ61/ZK60 joint. More secondary phases precipitated in the transition region near the AZ61 side than the ZK60 side.

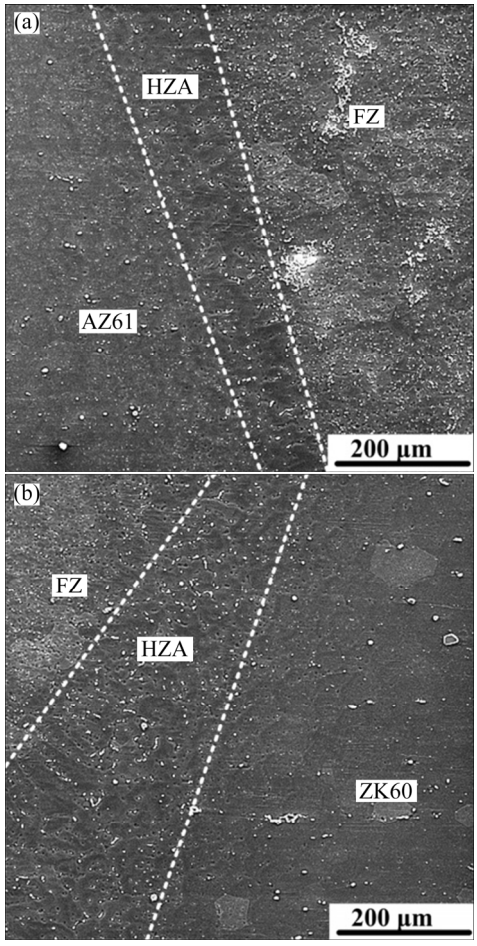

Fig. 8 Microstructural images of A-TIG welded AZ61/ZK60 magnesium alloy joints: (a) Transition zone near AZ61 base metal; (b) Transition zone near ZK60 base metal

The welding current of 80 A was chosen to examine the influence of TiO_2 on the welding of AZ61/ZK60 joints. Three different amounts of TiO_2 (5, 15 and 20 mg/cm^2) flux were pre-coated onto both sides of the AZ61 and ZK60 magnesium alloy plates with the width of 10 mm. The tensile strength, grain size, and weld beam width of the coated and uncoated joints were compared in Fig. 9. The tensile strength was inversely correlated with the amount of TiO_2 obviously due to the increased grain size in the FZ. The shape of the molten pool was randomly deflected following an increase in the coating amount while the width of the weld beam

decreased compared to the uncoated samples. Increases in the amount of TiO_2 resulted in increased arc shrinking and decreased welded beam width. With the increase of TiO_2 amounts, the heat dissipation suppressed in the weld beams, then the FZ grains were coarsened and the tensile strength of the welded joints was deceased. The TiO_2-coated samples exhibited a maximum tensile strength of 156 MPa, which was 24.5% lower than that of the uncoated samples (207 MPa). In addition, the tensile fracture across the fusion zone of the A-TIG welded AZ61/ZK60 joints indicated that a relatively uniform microstructure of the joint formed because of the vigorous stirring of the molten pool. Therefore, the formation of uneven heat-affected zone had no significant effect on the overall joint performances.

The SEM images of the typical tensile fracture surfaces of the AZ61 magnesium alloy, the ZK60 magnesium alloy, the TIG welded joint (80 A) and the A-TIG welded joint (80 A) are shown in Fig. 10. The fracture surface of the base metals (AZ61 and ZK60) mainly exhibited the features of ductile fracture, which was characterized by the formation of dimples and

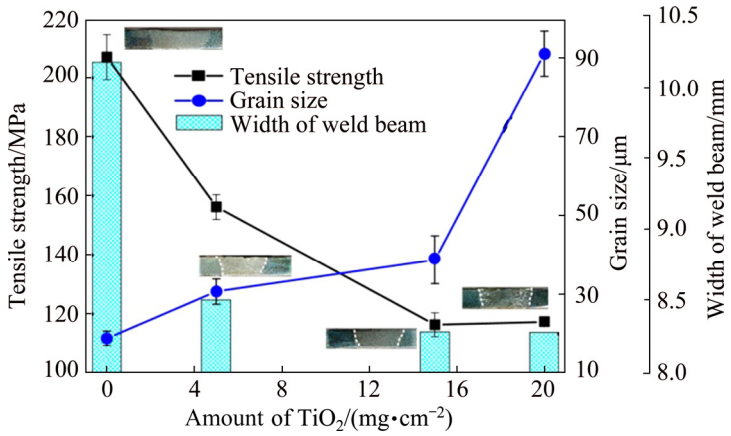

Fig. 9 Tensile strength, grain size of FZ, and width of weld beam of A-TIG welded joint with different amounts of TiO_2 additions

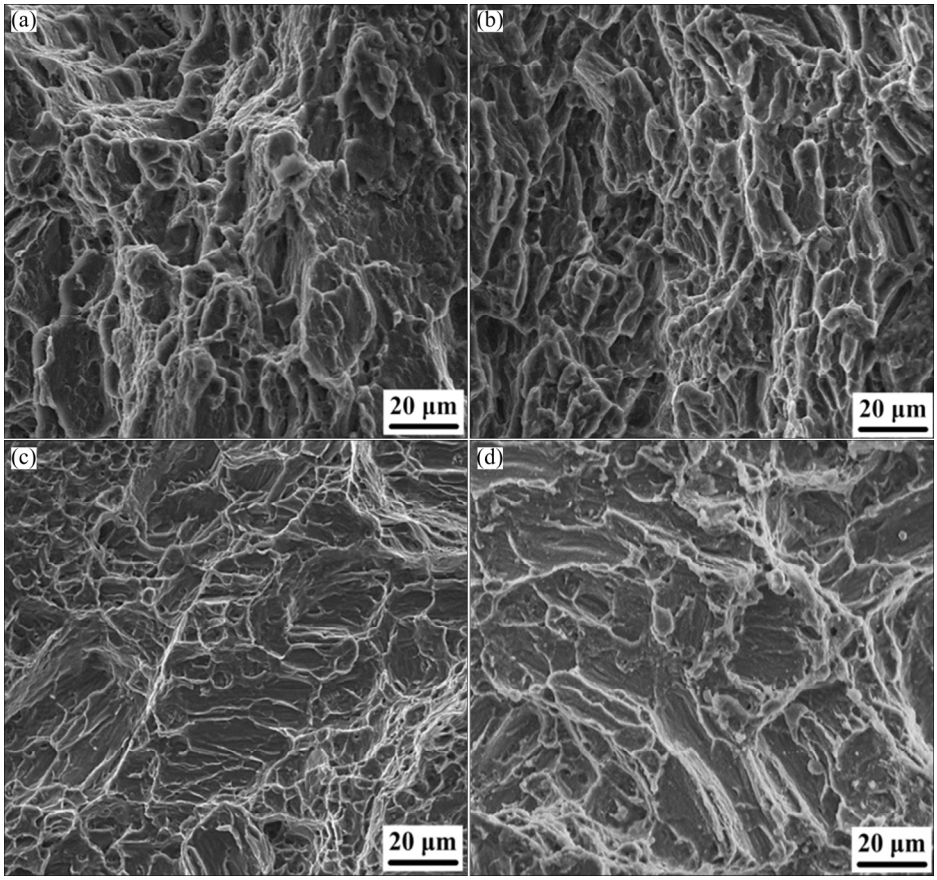

Fig. 10 SEM images of tensile fractured surfaces: (a) AZ61 base metal; (b) ZK60 base metal; (c) TIG welded joints; (d) A-TIG welded joints

tearing fibers. Both cleavage surfaces and dimples were observed in the welded joints, which had typical mixed-fracture features. The observed fracture of the TIG welded AZ61/ZK60 magnesium alloy joint indicated that it suffered both ductile and brittle deformation during the tensile tests. Obviously, the fracture of TIG welded joint was located in the HAZ as it is the weakest zone in the TIG welded joint of the magnesium alloy. Due to the thermal cycling effect, the grain coarsening in the HAZ resulted in a decrease in the tensile strength of the welded joint. Furthermore, the local stress concentrations were generated in the HAZ by the secondary phase particles along the grain boundaries [24], which suggested that the possible initiation of cracks formed at the brittle secondary phase along the grain boundaries. Similar mixed fracture features were observed in the fracture surface of the A-TIG welded joint due to the coarsening of the grains with distinct cleavage fracture morphology and the presence of the TiO_2 particles.

4 Conclusions

(1) Both $Mg_{17}Al_{12}$ and $MgZn_2$ particles were observed in the microstructures of the fusion zone, which was incorporated with the fine α-Mg equiaxed dendrite crystals. The volume fractions of the $Mg_{17}Al_{12}$ and $MgZn_2$ particles in the central fusion zone were similar. Moreover, the distance from the central fusion zone was inversely correlated with the volume fraction of the secondary phase particles.

(2) For the TIG welded AZ61/ZK60 joints, a refined grain size of 19 μm and a maximum tensile strength of 207 MPa were achieved at a welding current of 80 A. The tensile strength of the AZ61/ZK60 joints was inversely correlated to the amount of TiO_2 in A-TIG welding. The TiO_2-coated samples (5 mg/cm^2) exhibited a maximum tensile strength of 156 MPa.

(3) The TIG/A-TIG welded AZ61/ZK60 magnesium alloy joints did not present any obvious performance inhomogeneity due to molten pool stirring. However, narrower weld beam was observed with the increase of TiO_2 amount in A-TIG welding.

References

[1] MIN Dong, SHEN Jun, LAI Shi-qiang, JIE Chen, NAN Xu, HUI Liu. Effects of heat input on the low power Nd: YAG pulse laser conduction weldability of magnesium alloy AZ61 [J]. Optics and Lasers in Engineering, 2011, 49: 89−96.

[2] MORDIKE B L, EBERT T. Magnesium: Properties−applications−potential [J]. Materials Science & Engineering A, 2001, 302: 37−45.

[3] WAN Xiao-feng, SUN Yang-shan, XUE feng, BAI Jing, TAO Wei-jian. Microstructure and mechanical properties of ZA62 based magnesium alloys with calcium addition [J]. Transactions of Nonferrous Metals Society of China, 2010, 20: 757−762.

[4] HUANG Xin-sheng, YASUMASA C, MOTOHIRO Y, HIRONORI U, MASASHI I, FUTOSHI K, TOSHIHARU M. Microstructure and mechanical properties of AZX912 magnesium alloy extruded at different temperatures [J]. Materials Science & Engineering A, 2017, 679: 162–171.

[5] ZHANG Da-tong, MAYUMI S, KOUICHI M. Microstructural evolution of a heat-resistant magnesium alloy due to friction stir welding [J]. Scripta Materialia, 2005, 52: 899–903.

[6] GAO M, ZENG X Y, TAN B, FENG C. Study of laser MIG hybrid welded AZ31 magnesium alloy [J]. Science and Technology of Welding & Joining, 2013, 14(4): 274–281.

[7] ZHANG Tao, SHEN Jun, LV Lu-qiang, WANG Chun-min, SANG Jia-xin, WU Dong. Effects of graphene nanoplates on microstructures and mechanical properties of NSA-TIG welded AZ31 magnesium alloy joints [J]. Transactions of Nonferrous Metals Society of China, 2017, 27: 1285−1293.

[8] HOU Zhong-lin, LIU Li-ming, LV Xin-ze, QIAO Jun, WANG Hong-yang. Numerical simulation for pulsed laser–gas tungsten arc hybrid welding of magnesium alloy [J]. Journal of Iron & Steel Research International, 2018, 25(9): 995−1002.

[9] LIU Hong-tao, ZHOU Ji-xue, ZHAO Dong-qing, LIU Yun-teng, WU Jian-hua, YANG Yuan-sheng, MA Bai-chang, ZHUANG Hai-hua. Characteristics of AZ31 Mg alloy joint using automatic TIG welding [J]. International Journal of Minerals Metallurgy & Materials, 2017, 24: 102−108.

[10] SEVVEL P, JAIGANESH V. Impact of process parameters during friction stir welding of AZ80A Mg alloy [J]. Science & Technology of Welding & Joining, 2016, 21: 83−90.

[11] SHEN Jun, WEN Li-biao, LI Yang, MIN Dong. Effects of welding speed on the microstructures and mechanical properties of laser welded AZ61 magnesium alloy joints [J]. Materials Science & Engineering A, 2013, 578: 303−309.

[12] CARLONE P, ASTARITA A, RUBINO F, PASQUINO N. Microstructural aspects in FSW and TIG welding of cast ZE41A magnesium alloy [J]. Metallurgical & Materials Transactions B, 2016, 47: 1−7.

[13] ATABAKI M M, MA J, LIUW, KOVACEVIC R. Hybrid laser/arc welding of advanced high strength steel to aluminum alloy by using structural transition insert [J]. Materials & Design, 2015, 75: 120−135.

[14] XU C, SHENG G, WANG H, YUAN X. Reinforcement of Mg/Ti joints using ultrasonic assisted tungsten inert gas welding–brazing technology [J]. Science and Technology of Welding & Joining, 2014, 19: 703−707.

[15] SHEN Jun, XU Nan. Effect of preheat on TIG welding of AZ61 magnesium alloy [J]. International Journal of Minerals Metallurgy and Materials, 2012, 19(4): 360−363.

[16] WEN Tong, LIU Shi-yao, CHEN Shi, LIU Lan-tao, YANG Chen. Influence of high frequency vibration on microstructure and mechanical properties of TIG welding joints of AZ31 magnesium alloy [J]. Transactions of Nonferrous Metals Society of China, 2015, 25(2): 397−404.

[17] YANG Fang-zhou, ZHOU Jie, DING Rong-rong. Ultrasonic vibration assisted tungsten inert gas welding of dissimilar magnesium alloys [J]. Journal of Materials Science & Technology, 2018, 34: 2240−2245.

[18] SONG Gang, DIAO Zhuo, LV Xin-ze, LIU Li-ming. TIG and laser–TIG hybrid filler wire welding of casting and wrought dissimilar magnesium alloy [J]. Journal of Manufacturing Processes, 2018, 34: 204−214.

[19] TEMPLEMAN Y, HAMU G B, MESHI L. Friction stir welded AM50 and AZ31 Mg alloys: Microstructural evolution and improved corrosion resistance [J]. Materials Characterization, 2017, 126: 86−95.

[20] YANG Z, LI J P, GUO Y C, LIU T, XIA F, ZENG Z W, LIANG M X. Precipitation process and effect on mechanical properties of Mg−9Gd−3Y−0.6Zn−0.5Zr alloy [J]. Materials Science & Engineering A, 2007, 454: 274−280.

[21] LIU F, SOMMER F, BOS C, MITTEMEIJER E J. Analysis of solid state phase transformation kinetics: Models and recipes [J]. Metallurgical Reviews, 2007, 52: 193−212.

[22] SHI Lai-xin, SHEN Ping, ZHANG Dan, JIANG Qi-chuan. Wetting and evaporation behaviors of molten Mg–Al alloy drops on partially oxidized α-SiC substrates [J]. Materials Chemistry & Physics, 2011, 256: 7043−7047.

[23] ZHANG R F, SHENG S H, LIU B X. Predicting the formation enthalpies of binary intermetallic compounds [J]. Chemical Physics Letters, 2007, 442(4): 511−514.

[24] MUNITZ A, COTLER C, STERN A, KOHN G. Mechanical properties and microstructure of gas tungsten arc welded magnesium AZ91D plates [J]. Materials Science & Engineering A, 2001, 302: 68−73.

AZ61/ZK60 异种镁合金 TIG 与 A-TIG 接头的组织及力学性能

覃 波[1,2]，尹付成[1]，曾承宗[3]，谢佳成[3]，沈 骏[3]

1. 湘潭大学 材料科学与工程学院，湘潭 411105；
2. 湖南工程学院 汽车动力与传动系统湖南省重点实验室，湘潭 411104；
3. 重庆大学 材料科学与工程学院 国家镁合金材料工程技术研究中心，重庆 400044

摘 要：采用钨极氩弧(TIG)焊与活性钨极氩弧(A-TIG)焊对异种镁合金 AZ61/ZK60 进行焊接。结果发现，焊接接头主要由细小的等轴树枝晶与 $Mg_{17}Al_{12}$、$MgZn_2$ 颗粒组成。当焊接电流为 80 A 时，接头晶粒细化程度最大，晶粒尺寸为 19 μm，抗拉强度达到 207 MPa。使用 A-TIG 焊获得的异种镁合金接头抗拉强度和焊缝宽度与焊接前 TiO_2 活性剂涂敷量有关，焊缝两侧不同母材导致的热影响区组织差异并不影响焊缝成型。

关键词：AZ61；ZK60；异种接头；钨极氩弧(TIG)焊；活性钨极氩弧(A-TIG)焊；不均匀性

(Edited by Bing YANG)